72-Hz refresh we used an antialiasing algorithm in which each 13.8-ms frame of a movie was constructed by averaging 14 images representing the position of the CRF at about 1-ms resolution.

11. All animal procedures were approved by the University of California, Berkeley, Animal Care and Use Committee and conformed to or exceeded all relevant National Institutes of Health and U.S. Department of Agriculture standards. Single neuron recordings were made from two awake, behaving macaque monkeys (*Macaca mulatta*) with extracellular electrodes. Additional details about recording and surgical procedures are given in [C. E. Connor *et al.*, *J. Neurosci.* **17**, 3201 (1997)]. All data reported here were taken under conditions of excellent single-unit isolation. Eye position was monitored with a scleral search coil and trials were aborted if the eye deviated from fixation by more than 0.35°. Movie duration varied from 5 to 10 s. During recording sessions each movie was divided into 5-s segments; segments were then shown in and around the CRF on successive trials while the animal performed a fixation task for a juice reward. Each trial consisted of a stimulus of a single size with differently sized stimulus conditions randomly interleaved across trials.
12. A well-established and useful description of how sparsely a neuron responds across stimuli is given by its activity fraction, $A = (\Sigma r_i/n)^2/\Sigma(r_i^2/n)$. For further discussion see [E. T. Rolls and M. J. Tovee, *J. Neurophysiol.* **73**, 713 (1995)]. Our sparseness statistic is a convenient rescaling of A that ranges from 0% to 100%: $S = (1 - A)/(1 - A_{MIN}) = (1 - A)/(1 - 1/n)$.
13. Throughout this report we measured significance with randomization tests using 1000 random permutations of the relevant data. For further discussion see [B. F. J. Manly, *Randomization and Monte-Carlo Methods in Biology*, (Chapman & Hall, New York, 1991)].
14. If responses are averaged within a fixation, sparseness declines from 41 to 23%, 52 to 34%, 61 to 42%, and 62 to 45% for stimuli one, two, three, and four times the size of the CRF, respectively.
15. The boundaries of the CRF were estimated with bar and grating stimuli whose characteristics were controlled interactively. For 38 of 61 neurons we confirmed these manual estimates by reverse correlation on responses evoked by a dynamic sequence of small white squares distributed in and around the CRF (square positions were chosen randomly for each frame). Reliable CRF estimates were obtained with 150 to 300 s of data (30 to 60 behavioral fixation trials). Generally there is excellent agreement between the CRF profile estimates obtained with the two methods. Our CRF estimates ranged from about 20 to 50 min of arc, which is entirely consistent with the range of receptive field diameters obtained in awake behaving macaques by other researchers; for example, see [D. M. Snodderly and M. Gur, *J. Neurophysiol.* **74**, 2100 (1995)].
16. S. J. Judge, R. H. Wurtz, B. J. Richmond, *J. Neurophysiol.* **43**, 1133 (1980); B. C. Motter, *J. Neurophysiol.* **70**, 909 (1993).
17. Animals viewed high-resolution natural images digitized on commercial photo-CDs (Corel Corp.) and shown at a resolution of 1280 × 1024 pixels. Images were shown for 10 s each. Neural responses and eye position were recorded continuously during this free viewing (*8*). Natural vision movies that simulated these specific free-viewing episodes were constructed by using the eye position records to determine the position of the recorded CRF during free viewing. In six cells the diameter of the reconstructed movies was four times the CRF, and in 11 cells it was three times the CRF. These data have been combined in this report.
18. Each free-viewing episode produced a single-spike train evoked by a unique pattern of exploratory eye movements. In contrast, natural vision movies were repeated many times. To obtain comparable sparseness estimates for these data, we separately analyzed the spike train evoked by each repetition of the natural vision movie. The average of this distribution of sparseness values was then compared with the single sparseness value obtained from the free-viewing data. To ensure matched stimulus conditions, we made all comparisons on a movie-by-movie basis. Note that sparseness values based on single-spike trains are biased upward because of the discrete nature of spike generation.
19. The random sinusoidal grating sequence was similar to that used by D. L. Ringach, M. J. Hawken, R. Shapley [*Nature* **387**, 281 (1997)]. The orientation, spatial frequency, and phase of the grating were chosen randomly on each video frame (at 72 Hz). Gratings were shown at a Michelson contrast of 0.5. Before analysis, stimuli were binned into 10° orientation steps and 6 to 12 spatial frequency steps. Responses were analyzed by parametric reverse correlation on orientation and spatial frequency, averaging over phase. The mean responses across stimulus bins (at the peak response latency) were used to estimate the sparseness statistic.
20. A. J. Bell and T. J. Sejnowski, *Vision Res.* **37**, 3327 (1997).
21. Several theoretical studies of sparse population coding have reported the kurtosis of the distribution of responses observed across a set of linear filters, with respect to a particular stimulus ensemble (*2, 20*). This measure is not directly applicable to our data because the responses of area V1 neurons are asymmetric: cells typically exhibit low spontaneous rates and appropriate stimuli elevate these rates. To estimate kurtosis we converted each response distribution to a symmetric distribution by reflecting the data about the origin. The resulting symmetric distributions are unimodal with zero mean and decrease smoothly to zero. Our kurtosis statistic is well behaved and directly comparable to the results of theoretical studies.
22. Let P_1 and P_2 be the PSTH response vectors for a pair of neurons. Then $\cos(\theta) = P_1P_2/\|P_1\| \times \|P_2\|$, where $\|P_n\|$ is the norm of the appropriate vector. This measure is sensitive to changes across the basis dimensions of the movie time stream and is insensitive to differences in absolute rate.
23. It is difficult to choose a scalar measure of response similarity appropriate for all situations; see [P. Di Lorenzo, *J. Neurophysiol.* **62**, 823 (1989)]. To validate our results we performed two alternative versions of the population decorrelation analysis. For each neuron pair we also computed both the linear correlation coefficient and the neural discrimination index of Di Lorenzo. In both cases, nCRF stimulation leads to significant decorrelation ($P \leq 0.001$). To ensure that the slightly different stimulus sizes do not influence our results, we also performed all similarity analyses on a data set restricted to neuron pairs with identical CRF sizes (and thus identical stimulation). Under these conditions the decorrelating effect of the nCRF remains significant ($P \leq 0.001$).
24. The compound grating stimulus consisted of a CRF conditioning grating and a probe grating. We set the conditioning grating's orientation and spatial frequency to the neuron's preferred values [as determined by reverse correlation on responses to a dynamic grating sequence (*19*) presented in the CRF]. The phase of the conditioning grating varied randomly with each video frame. Both gratings were presented at a Michelson contrast of 0.5 and their edges were blended into one another and into the background. We performed reverse correlation on the position of the probe grating within the nCRF annulus (collapsing over all other parameters). To measure baseline responses we presented interleaved trials containing only the conditioning grating.
25. G. A. Walker *et al.*, *J. Neurosci.* **19**, 10536 (1999).
26. Y. Dan, J. J. Atick, R. C. Reid, *J. Neurosci.* **16**, 3351 (1996).
27. M. S. Lewicki and B. A. Olshausen, in *Advances in Neural Information Processing Systems 10*, M. I. Jordan, M. J. Kearns, S. A. Solla, Eds. (MIT Press, Cambridge, MA, 1997) pp. 815–821.
28. D. J. Heeger, *Visual Neurosci.* **9**, 181 (1992); C. D. Gilbert, *Neuron* **9**, 1 (1992); A. M. Sillito *et al.*, *Nature* **378**, 492 (1995); C. D. Gilbert *et al.*, *Proc. Natl. Acad. Sci. U.S.A.* **93**, 615 (1996); M. Carandini *et al.*, *J. Neurosci.* **17**, 8621 (1997); J. J. Knierim and D. C. Van Essen, *J. Neurophysiol.* **67**, 961 (1992).

20 August 1999; accepted 27 December 1999

Mitochondrial FtsZ in a Chromophyte Alga

Peter L. Beech,[1,3]* Thao Nheu,[3]† Thomas Schultz,[3]‡ Shane Herbert,[1] Trevor Lithgow,[4] Paul R. Gilson,[2,3] Geoffrey I. McFadden[2,3]

A homolog of the bacterial cell division gene *ftsZ* was isolated from the alga *Mallomonas splendens*. The nuclear-encoded protein (MsFtsZ-mt) was closely related to FtsZs of the α-proteobacteria, possessed a mitochondrial targeting signal, and localized in a pattern consistent with a role in mitochondrial division. Although FtsZs are known to act in the division of chloroplasts, MsFtsZ-mt appears to be a mitochondrial FtsZ and may represent a mitochondrial division protein.

Mitochondria are ubiquitous organelles that form networks, reticulae, or punctate structures in eukaryotic cells. Mitochondria in many cells appear to constitutively fuse with one another and divide (*1*), but we know little about the proteins involved in these processes, particularly mitochondrial division. Eukaryotes depend on mitochondria for respiration and adenosine triphosphate synthesis and rely on them to divide before daughter mitochondria can be apportioned to each new cell generation. In chloroplasts, homologs of the bacterial cell division protein FtsZ are essential components of the organellar division machinery (*2*). FtsZ is found in nearly all prokaryotes, is structurally related to tubulin, and accumulates at the furrow between dividing cells, playing a critical role in cell division (*3*). No potential mitochondrial FtsZ has been identified in the complete genomes of *Caenorhabditis elegans* or *Saccharomyces cerevisiae*. However, because both mitochondria and chloroplasts arose from endosymbiotic bacteria, we anticipated that early in evolution, mitochondrial division might also have been regulated by FtsZ. Here we de-

scribe two distinct complementary DNAs for FtsZ homologs from an algal flagellate: One appears to encode an FtsZ of the chloroplast, and the second appears to encode an FtsZ of the mitochondrion.

We screened a cDNA library of the unicellular chromophyte (stramenopile) alga *Mallomonas splendens* (*4*) with two probes: (i) part of the chloroplast *AtFtsZ1-1* gene of the plant *Arabidopsis thaliana* (*5*) and (ii) a fragment of the *ftsZ1* gene of the α-proteobacterium *Sinorhizobium meliloti* (*6*). The screens recovered two cDNAs, and Southern blot analyses confirmed that each corresponded to a different, single-copy, nuclear gene in *M. splendens*. The *Arabidopsis* probe detected a *Mallomonas ftsZ* homolog that we call *MsFtsZ-cp* (*Mallomonas splendens FtsZ–chloroplast*; GenBank accession number AF120117), because sequence analysis showed a translation product with clear affinities to other known chloroplast FtsZ proteins. MsFtsZ-cp was unequivocally allied to chloroplast FtsZs from the red algae *Cyanidium* and *Galdieria*, the cryptomonad alga *Guillardia*, the plants *Arabidopsis* and pea, and the moss *Physcomitrella*, which in turn are related to FtsZs of cyanobacteria, from which chloroplasts derive (Fig. 1). We thus believe that MsFtsZ-cp has a role in dividing the *Mallomonas* chloroplast.

The second screen, probing for sequences related to the α-proteobacterial gene, identified a second *Mallomonas ftsZ* homolog, which we call *MsFtsZ-mt* (*Mallomonas splendens FtsZ–mitochondrion*; GenBank accession number AF120116). Phylogenetic analyses (Fig. 1) of the predicted 401–amino acid protein (relative molecular mass 42310) demonstrated that MsFtsZ-mt was most closely related to FtsZs of α-proteobacteria—the nearest known bacterial relatives of mitochondria (*7*). Northern blot analysis revealed a *MsFtsZ-mt* transcript of the expected size (~1.25 kb) in mRNA isolated from asynchronous cultures of *M. splendens*. MsFtsZ-mt has an NH_2-terminal extension predicted to act as a basic, amphipathic, mitochondrial targeting sequence (*8*).

The mitochondria of *M. splendens* are, like those of most other cells, highly plastic and dynamic (*1*, *9*). At any one time, they number 15 to 30 per cell and can rapidly (over several seconds) change shape between being spherical, ellipsoid, elongate, or platelike. They move within the cell and undergo frequent fission and fusion events (*10*). Viewed within living cells at interphase, at least one mitochondrion (usually several) is medially constricted (Fig. 2B shows examples in fixed cells), and these dividing mitochondria become completely separated within 1 min (*10*). Observations of the fusion of mitochondria (*10*) suggest that the tip of one mitochondrion meets and fuses with the end or side of a second mitochondrion, similar to mitochrondrial fusion, in other eukaryotes (*1*, *9*).

To determine the location of MsFtsZ-mt in *M. splendens*, we generated antisera to bacterially expressed protein (*11*) (Fig. 2A). Confocal microscopy of immunolabeled interphase cells (Fig. 2, B through I) showed that MsFtsZ-mt was always associated with mitochondria and displayed patches of labeling in two distinct locations: around the middle of mitochondria (medial localization) and at the edges of mitochondria (peripheral localization). Medial localization was often associated with mitochondria that were constricted (arrowheads, Fig. 2D) and possibly represented MsFtsZ-mt in dividing organelles, similar to the localization of FtsZ in dividing bacteria (*3*). A series of confocal sections showed three mitochondria, each with a medial belt of anti–MsFtsZ-mt labeling (Fig. 2, E through I); although these mitochondria were not obviously constricted, they may have been in the very early stages

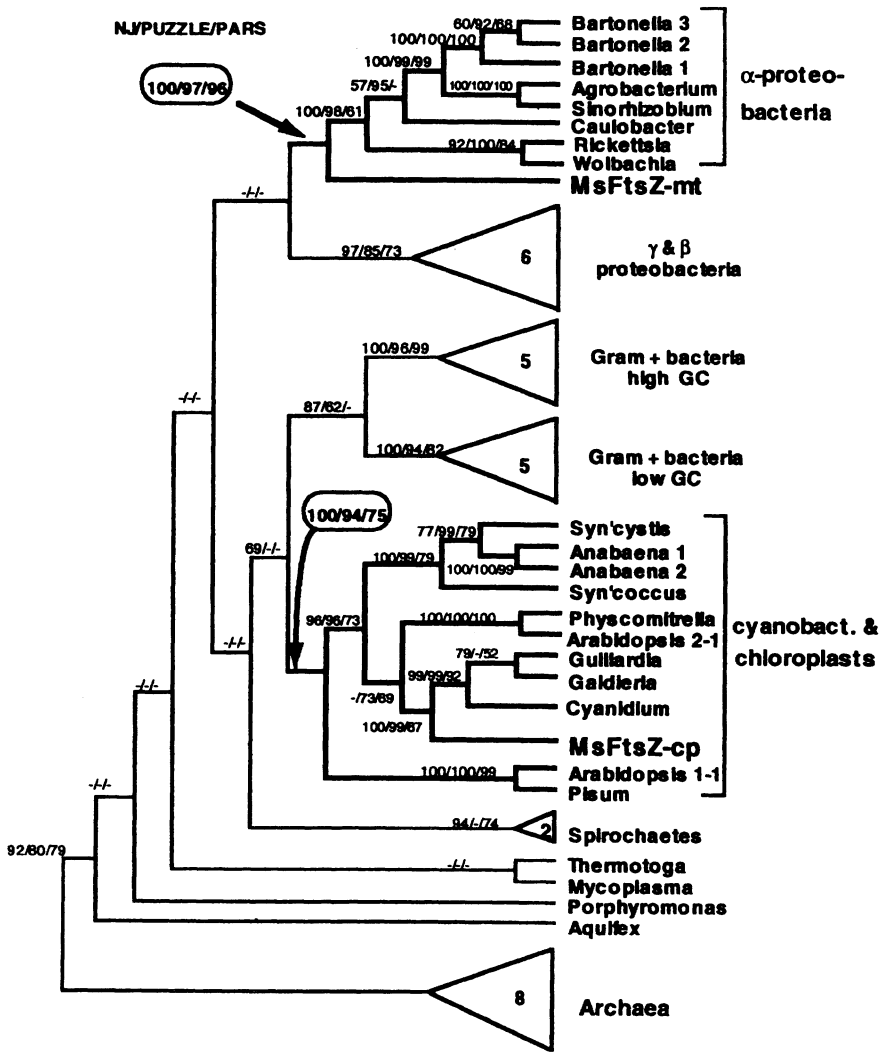

Fig. 1. Phylogeny of FtsZ showing the position of the two *Mallomonas* proteins. Major bacterial groups are represented as triangles, with the number of taxa therein. The *Mallomonas* chloroplast FtsZ (MsFtsZ-cp) is allied with other algal chloroplast FtsZs (*Galdieria*, *Cyanidium*, and *Guillardia*) with very high levels of confidence. The *Mallomonas* mitochondrial FtsZ (MsFtsZ-mt) is unequivocally the sister to α-proteobacteria, the group from which mitochondria derive. This is a quartet puzzling tree for 52 sequences with 306 sites. Numbers at the nodes refer to percentage bootstrap support in distance, frequency in 1000 quartet puzzling replicates, and percentage bootstrap support in parsimony (Paup 4.0b2a). Dashes at the nodes of the tree indicate less than 50% support. Alignment and accession numbers are available on request.

[1]Centre for Cellular and Molecular Biology, School of Biological and Chemical Sciences, Deakin University, 221 Burwood Highway, Melbourne, 3125, Australia. [2]Plant Cell Biology Research Centre, [3]School of Botany, [4]Department of Biochemistry and Molecular Biology, University of Melbourne, 3010, Australia.

*To whom correspondence should be addressed. E-mail: plbeech@deakin.edu.au

†Present address: Ludwig Institute for Cancer Research, Royal Melbourne Hospital, 3050, Australia.

‡Present address: The Scripps Research Institute, 11055 North Torrey Pines Road, La Jolla, CA 92037, USA.

of division. In bacteria, the FtsZ ring forms before there are any morphological indicators (such as cell shape) of division (*12*). Peripheral localization of MsFtsZ-mt (arrows, Fig. 2D) appeared as one to several patches per mitochondrion and often occurred at mitochondrial poles. The similarities between the localization of MsFtsZ-mt in *M. splendens* and the behavior of bacterial FtsZ suggest that MsFtsZ-mt acts in mitochondrial division. Furthermore, the distribution of MsFtsZ-mt is strikingly similar to that shown by Dnm1, a dynamin-related guanosine triphosphatase that regulates mitochondrial division in yeast and *C. elegans* (*13*). Dnm1 is found at the constricted regions of apparently dividing mitochondria (similar to the medial localization of MsFtsZ-mt) and at the ends of mitochondrial tubules that may have recently completed division (similar to some of the peripheral localizations of MsFtsZ-mt). However, Dnm1 and other dynamin-like proteins are located on the mitochondrial outer membrane (*13*, *14*), whereas MsFtsZ-mt has no predicted membrane-spanning domain and is likely to be transported to the inside of the mitochondrion.

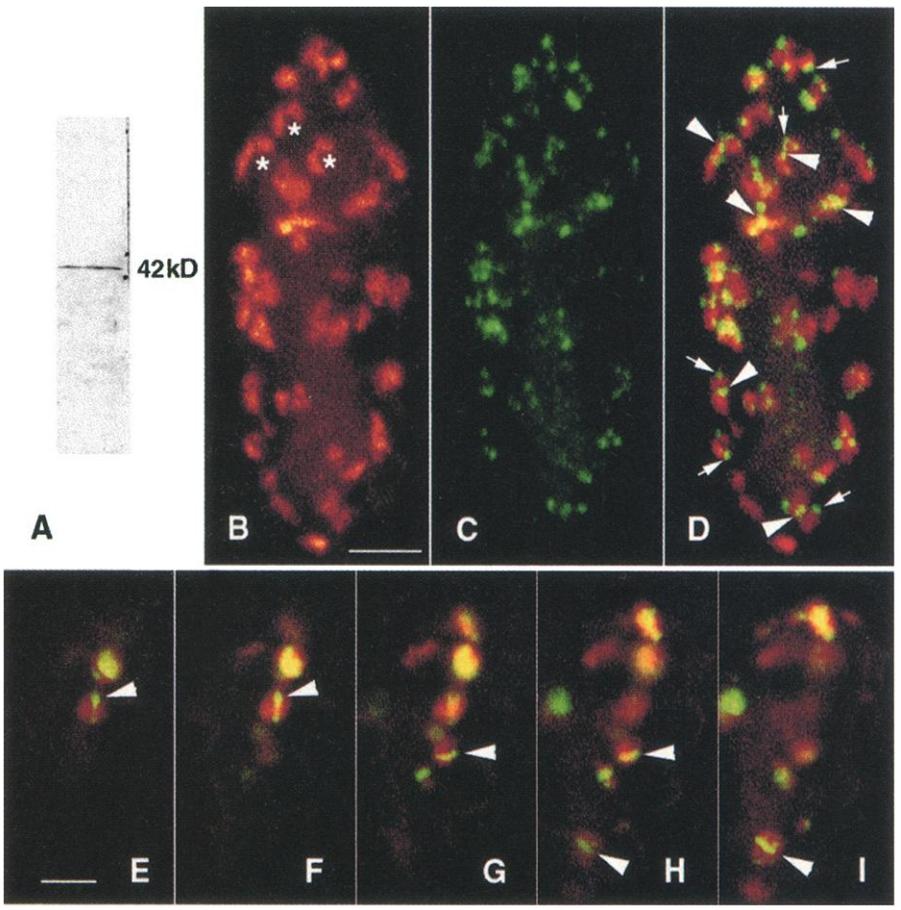

Fig. 2. Anti–MsFtsZ-mt labels protein associated with the mitochondria of *M. splendens*. (**A**) Western blot analysis of total cellular protein from *M. splendens* probed with anti–MsFtsZ-mt and detected with alkaline phosphatase–conjugated secondary antibodies is shown. The single immunoreactive band of ~42 kD is the expected size of the MsFtsZ-mt protein. (**B** through **I**) Confocal immunofluorescence microscopy of *M. splendens* (*17*, *18*) labeled with MitoTracker CMXRos [red channel (B)] and anti–MsFtsZ-mt [green channel (C)]; colocalization of mitochondria and anti–MsFtsZ-mt appears in yellow in the overlays of the two channels [(D) through (I)]. (B) through (D) show an entire cell. Three mitochondria that are medially constricted and possibly dividing are indicated by asterisks in (B). In (D), arrowheads and arrows indicate examples of medial and peripheral (respectively) anti–MsFtsZ-mt labeling of mitochondria. (E) through (I) are consecutive sections through part of a cell showing three mitochondria, each with a distinct medial belt of MsFtsZ-mt (arrowheads). Scale bars, 4 μm in (B) and 2 μm in (E).

To assess the submitochondrial localization of MsFtsZ-mt experimentally, the protein (including the putative mitochondrial targeting sequence) was expressed in yeast as a green fluorescent protein (GFP) fusion (*15*). Mitochondria purified from the transgenic yeast carried a protein corresponding in size to the MsFtsZ-mt fusion, and immunoblotting revealed MsFtsZ-mt within the mitochondrial compartment, not displayed on its surface (Fig. 3A). Confocal fluorescence microscopy showed that MsFtsZ-mt localized to yeast mitochondria (Fig. 3B), which exist as a reticulum around the cell cortex. The transgenic yeast appeared to have slightly abnormal mitochondrial morphologies: The mitochondria of most transformed cells displayed one or more bright nodes of fluorescence (Fig. 3, B, D, and E; of 100 cells, 68 had one node, 23 had two to four nodes, and 9 had no nodes of fluorescence), which were never observed in untransformed cells or in cells transformed with GFP targeted by fusion to other mitochondrial proteins.

If mitochondrial FtsZs are, in fact, absent from the genomes of all fungi and animals,

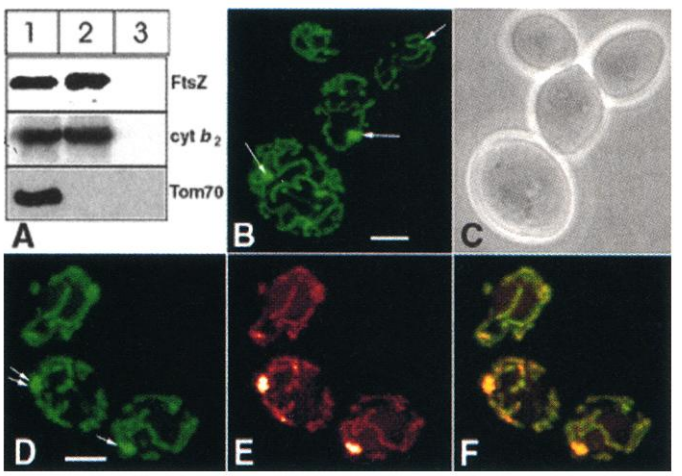

Fig. 3. *MsFtsZ-mt* cDNA tagged with GFP is targeted to the yeast mitochondrion. (**A**) Mitochondria were purified from yeast cells transformed with MsFtsZ-mt/GFP, subjected to limited proteolysis with trypsin, and then analysed by SDS–polyacrylamide gel electrophoresis and immunoblotting (*15*). With an antibody to GFP, MsFtsZ-mt/GFP (FtsZ) was detected in mitochondria (lane 1) and in mitochondria treated with trypsin (lane 2), but was degraded by trypsin when the membranes were ruptured by osmotic shock (lane 3). Control immunoblots reveal the fate of the surface-located protein Tom70 and the intermembrane space protein cyt b_2. (**B** through **F**) Confocal fluorescence microscopy (*17*) of yeast cells transformed with the MsFtsZ-mt/GFP fusion. (B) and (D) show green fluorescence from the MsFtsZ-mt/GFP fusion; arrows indicate bright nodes of fluorescence in the mitochondria. (C) is the corresponding phase contrast image of (B). (E) shows co-staining of the cells in (D) with the mitochondrial-specific dye Mitotracker CMXRos (Molecular Probes) as described (*9*). (F) is the overlay of (D) and (E) revealing (in yellow) colocalization of the MsFtsZ-mt/GFP fusion with mitochondria. Scale bars, 2 μm.

then it is possible that the dynamin-like proteins have taken over the role of FtsZ in mitochondrial division in these organisms. However, MsFtsZ-mt seems to be able to affect mitochondrial morphology even in an organism such as yeast that normally relies on Dnm1 for organelle division. It seems likely that there will be major mechanistic differences in mitochondrial fission catalyzed by dynamins or FtsZs: one protein working from the outside of the organelle and the other from the inside.

We conclude that *MsFtsZ-mt* is likely to have been acquired from an endosymbiotic α-proteobacterium that was the ancestor of the present-day mitochondrion. We suggest that in the course of evolution, the gene was transferred from mitochondrion to nucleus (*16*) and that the nuclear-encoded protein is now targeted back to the mitochondrion to play a role in the division of the organelle. This is the first identification of a eukaryotic *ftsZ* whose protein seems to be specifically targeted to the mitochondrion, and which may thus be related to the earliest mitochondrial division genes. The *Mallomonas* mitochondrial FtsZ will be a useful key for identifying other components critical to moulding the shape and facilitating the intergenerational transmission of mitochondria.

Note added in proof: A possible mitochondrial FtsZ from a red alga has recently been reported. The predicted protein of *CmftsZ1* (GenBank accession number AB032071) is 53% identical to MsFtsZ-mt and clusters with MsFtsZ-mt and the proteobacteria in a phylogenetic analysis like that in Fig. 1.

References and Notes

1. J. Bereiter-Hahn and M. Vöth, *Microsc. Res. Tech.* **27**, 198 (1994); K. P. Gaffal, *Endocyt. Cell Res.* **4**, 41 (1987).
2. K. W. Osteryoung and E. Vierling, *Nature* **376**, 473 (1995); K. W. Osteryoung, K. D. Stokes, S. M. Rutherford, A. L. Percival, W. Y. Lee, *Plant Cell* **10**, 1991 (1998); R. Strepp, S. Scholz, S. Kruse, V. Speth, R. Reski, *Proc. Natl. Acad. Sci. U.S.A.* **95**, 4368 (1998).
3. E. Bi and J. Lutkenhaus, *Nature* **354**, 161 (1991); D. Bramhill, *Annu. Rev. Cell Dev. Biol.* **13**, 395 (1997); H. P. Erickson, *Trends Cell Biol.* **7**, 362 (1997); J. Lutkenhaus and S. G. Addinall, *Annu. Rev. Biochem.* **66**, 93 (1997); J. Löwe and L. A. Amos, *Nature* **391**, 203 (1998); W. Margolin, *Trends Microbiol.* **6**, 233 (1998).
4. Polyadenylated RNA was extracted with phenol and chloroform from an asynchronously dividing culture of *M. splendens* [P. L. Beech and R. Wetherbee, *J. Phycol.* **26**, 90 (1990)] and used to construct a cDNA library with the help of a ZAP-cDNA Gigapack III Gold cloning kit (Stratagene).
5. Nucleotides 60 through 1265 of *AtFtsZ1-1* from *A. thaliana* (GenBank accession number U39877) were amplified by reverse transcription polymerase chain reaction from RNA isolated from leaves of *A. thaliana* (Columbia).
6. This second probe was a 535–base pair (bp) Nsi I–Mlu I fragment of the *ftsZ1* gene from *S. meliloti* (Genbank accession number M94386) [W. Margolin, J. Corbo, S. R. Long, *J. Bacteriol.* **173**, 5822 (1991)].
7. S. G. E. Andersson *et al.*, *Nature* **396**, 133 (1998); M. W. Gray, G. Burger, B. F. Lang, *Science* **283**, 1476 (1999).
8. The sequence of MsFtsZ-mt was e-mailed for analysis with the PSORT algorithm (http://psort.ims.u-tokyo.ac.jp). A mitochondrial targeting probability of 0.744 was predicted.
9. J. Nunnari *et al.*, *Mol. Biol. Cell* **8**, 1233 (1997).
10. This behavior was seen in unpublished observations by P. L. Beech on live cells of *M. splendens* labeled with Mitotrackers Green FM or CMXRos (Molecular Probes) according to the manufacturer's instructions.
11. An Eco RI–Spe I fragment (representing amino acids 8 through 342) of the *MsFtsZ-mt* cDNA was cloned into the ProEx HTb expression vector (Gibco). Six histidine fusion proteins were expressed in *Escherichia coli*, purified against Talon resin (Clontech), and electrophoretically separated before injection of gel slices into rabbits for antibody production. Antibodies likely to be specific to MsFtsZ-mt (anti–MsFtsZ-mt) were selected by affinity-purifying rabbit sera against the first 76 amino acids of MsFtsZ-mt [the corresponding cDNA fragment from *MsFtsZ-mt* was cloned into pGEX-4T-1 (Pharmacia) and expressed in *E. coli* as a glutathione *S*-transferase fusion protein] immobilized on nitrocellulose.
12. Q. Sun and W. Margolin, *J. Bacteriol.* **180**, 2050 (1998).
13. W. Bleazard *et al.*, *Nature Cell Biol.* **1**, 298 (1999); H. Sesaki and R. E. Jensen, *J. Cell Biol.* **147**, 699 (1999); A. M. Labrousse, M. D. Zappaterra, D. A. Rube, A. M. van der Bliek, *Mol. Cell* **4**, 815 (1999).
14. E. Smirnova, D.-L. Shurland, S. N. Ryazantsev, A. M. van der Bliek, *J. Cell Biol.* **143**, 351 (1998); K. A. Shepard and M. P. Yaffe, *J. Cell Biol.* **144**, 711 (1999); M. P. Yaffe, *Science* **283**, 1493 (1999).
15. Nucleotides –34 through 1157 of the 1203-bp *MsFtsZ-mt* cDNA open reading frame were inserted upstream of the GFP coding region on the centromeric plasmid p416MET25 that carried the GFP ($Ser^{65} \rightarrow Thr^{65}$) isoform. *S. cerevisiae* cells were transformed with the MsFtsZ-mt/GFP fusion as described [R. George *et al.*, *Proc. Natl. Acad. Sci. U.S.A.* **95**, 2296 (1998)]. Mitochondria were isolated and subfractionated as previously described [B. S. Glick *et al.*, *Cell* **69**, 809 (1992)].
16. J. D. Palmer, *Science* **275**, 790 (1997).
17. Cells were examined on a Leica TCS 4D laser scanning confocal microscope under a ×100 1.3 numerical aperture objective. Signals from green (GFP or fluorescein isothiocyanate) and red (Mitotracker) channels were collected simultaneously and merged with Adobe Photoshop.
18. For immunofluorescence, a nonsynchronously dividing culture of *M. splendens* was labeled with 100 nM MitoTracker CMX-Ros (Molecular Probes) for 2 hours; cells were washed in growth medium, then fixed in 2% paraformaldehyde in methanol at –20°C for 10 min, washed in phosphate-buffered saline (PBS), and labeled with primary antibody diluted in blocking buffer (PBS, 0.05% Tween-20, and 1% bovine serum albumin) overnight at 4°C. Primary antibodies were detected with FITC-conjugated goat anti-rabbit IgG (Selenius, Hawthorn, Victoria, Australia), and cells were observed as described (*17*). Seemingly identical labeling with anti–MsFtsZ-mt was achieved both with and without MitoTracker labeling. Controls for antibody labeling were performed with preimmune sera.

19. We thank W. Margolin for the *S. meliloti* FtsZ probe, C. Cobbett for *Arabidopsis* RNA, J. Pickett-Heaps and R. Wetherbee for materials and encouragement, and T. Spurck for help with confocal microscopy. P.L.B. is funded by the Australian Research Council and is a Queen Elizabeth II fellow.

9 November 1999; accepted 11 January 2000

Convergent Solutions to Binding at a Protein-Protein Interface

Warren L. DeLano,[1] Mark H. Ultsch,[2] Abraham M. de Vos,[2] James A. Wells[1*]

The hinge region on the Fc fragment of human immunoglobulin G interacts with at least four different natural protein scaffolds that bind at a common site between the C_{H2} and C_{H3} domains. This "consensus" site was also dominant for binding of random peptides selected in vitro for high affinity (dissociation constant, about 25 nanomolar) by bacteriophage display. Thus, this site appears to be preferred owing to its intrinsic physiochemical properties, and not for biological function alone. A 2.7 angstrom crystal structure of a selected 13–amino acid peptide in complex with Fc demonstrated that the peptide adopts a compact structure radically different from that of the other Fc binding proteins. Nevertheless, the specific Fc binding interactions of the peptide strongly mimic those of the other proteins. Juxtaposition of the available Fc-complex crystal structures showed that the convergent binding surface is highly accessible, adaptive, and hydrophobic and contains relatively few sites for polar interactions. These are all properties that may promote cross-reactive binding, which is common to protein-protein interactions and especially hormone-receptor complexes.

Protein-protein interactions are central to the control of many biological functions, but we do not yet understand what general features (if any) of a protein surface are most important for binding. Nature often provides convergent solutions to biological problems, and study of this "consensus" information can provide insight into the essential requirements for function. There are many examples of hormones that bind multiple receptors, or receptors that bind multiple hormones (*1*). Structural analysis of these complexes shows that the common protein will use virtually the same set of contact residues for binding many

[1]Graduate Group in Biophysics, University of California, San Francisco, CA 94143, USA and Sunesis Pharmaceuticals, 3696 Haven Avenue, Suite C, Redwood City, CA 94063, USA. [2]Department of Protein Engineering, Genentech, One DNA Way, South San Francisco, CA 94080, USA.

*To whom correspondence should be addressed. E-mail: jaw@sunesis-pharma.com